microorganisms

MDPI

Article

Siderophore-Producing Bacteria from the Santiago River: A Quantitative Study and Biocomposite Applications

Mariana R. Corona-Ramírez [1], Nidia N. García-Valdez [2], Luis A. Romero-Cano [1], Camila S. Gómez-Navarro [1], Ma Isidora Bautista-Toledo [3], Francisco Carrasco-Marín [3], Fabiola Padilla-Arizmendi [4], Karina Sandoval-García [2,5,*] and Marco A. Zárate-Navarro [1,*]

1 Grupo de Investigación en Materiales y Fenómenos de Superficie, Departamento de Biotecnológicas y Ambientales, Universidad Autónoma de Guadalajara, Av. Patria 1201, Zapopan C.P. 45129, Jalisco, Mexico
2 Departamento de Biotecnológicas y Ambientales, Universidad Autónoma de Guadalajara, Av. Patria 1201, Zapopan C.P. 45129, Jalisco, Mexico
3 UGR-Carbon, Materiales Polifuncionales Basados en Carbono, Departamento de Química Inorgánica, Facultad de Ciencias, Unidad de Excelencia Química Aplicada a Biomedicina y Medioambiente, Universidad de Granada (UEQ-UGR), 18071 Granada, Spain
4 Dirección de Programas Académicos de Ciencias Químicas, Universidad Autónoma de Guadalajara, Av. Patria 1201, Zapopan C.P. 45129, Jalisco, Mexico
5 Centro Universitario de Ciencias Exactas e Ingenierías, Universidad de Guadalajara, Guadalajara C.P. 44430, Jalisco, Mexico
* Correspondence: karina.sandoval@edu.uag.mx (K.S.-G.); marco.zarate@edu.uag.mx (M.A.Z.-N.)

Abstract

The Santiago River near the Guadalajara Metropolitan Area is one of the most contaminated water bodies in Mexico, where heavy metals pose a major threat to aquatic ecosystems. Chronic metal pollution has promoted the adaptation of native microbial communities, including the production of metal-chelating metabolites such as siderophores, which represent a valuable resource for remediation-oriented biomaterials. In this study, bacterial strains were isolated from water and sediment samples, then screened for siderophore production using the Chrome Azurol S assay (CAS), complemented by a MATLAB-based image processing approach for semi-quantitative ranking prior to taxonomic identification by MALDI-TOF MS. Based on biosafety considerations and cultivation robustness, *Bacillus thuringiensis* was selected as a benchmark case, being immobilized onto activated carbon to produce a carbon–bacteria biocomposite (CBM). To evaluate the performance of CBM, Cu(II) was used as a model contaminant due to its industrial relevance, persistence, toxicity, and strong complexation behavior. Batch adsorption experiments showed that the CBM exhibited a 23.9% higher maximum Cu(II) sorption capacity than pristine activated carbon. Acute toxicity assays using Vibrio fischeri further indicated reduced toxicity in CBM-treated effluents, supporting the feasibility of this contained biocomposite for heavy metal remediation.

Keywords: Jalisco; Lerma–Chapala Basin; batch adsorption of copper; biosorption; *Bacillus thuringiensis*; carbon-based biocomposite

Academic Editor: Alejandro Rodriguez-Sanchez

Received: 19 December 2025
Revised: 22 January 2026
Accepted: 27 January 2026
Published: 5 February 2026

1. Introduction

The Santiago River in Jalisco, Mexico, is severely polluted due to rapid urbanization and intensive industrial activity, compounded by the lack of effective planning and contamination control policies [1]. Recent water quality characterizations have identified two major pollution hotspots: the urban fringe of Guadalajara—particularly the El Ahogado stream,

which receives massive industrial and municipal wastewater discharges—and the lower zone of the Verde River sub-basin. Their analysis reveals that pollutants such as ammonia, phosphorus, and heavy metals, including Fe, Al, Mn, B, Ba, Zn, As, Cu, Cr, Ni, Pb, and Cd, frequently exceed maximum permissible limits by orders of magnitude (Figure A1a shows, as an example, the historical trend of Fe concentrations from 2009 to 2025, highlighting the complexity of the pollution problem), together with elevated chemical oxygen demand (COD) values [2]. Nonetheless, the study also recognizes a significant natural attenuation capacity downstream, where pollutant concentrations are partially reduced through dilution from tributaries and rainfall, as well as through the sediment-trapping effect of dams (Figure A1b).

Under these extreme environmental conditions, native bacterial communities have adapted through ecological selection processes. Bacterial communities in heavy metal-contaminated environments exhibit enhanced siderophore production along natural contamination gradients and in controlled microcosm experiments [3,4]. This increased production facilitates environmental detoxification by enabling the extracellular sequestration of toxic metals, such as copper, into stable siderophore–metal complexes that are unable to enter microbial cells, thereby reducing bioavailability and toxicity [5]. The selective advantage conferred by this mechanism is evidenced by a community shift toward high-producing genera and a correlated increase in metal tolerance among isolates, confirming that siderophore-mediated sequestration plays a critical role in mitigating metal stress in polluted soils [6–8].

Siderophores are secondary metabolites synthesized by non-ribosomal peptide synthetases that exhibit strong and structure-dependent affinity for ferric iron. These compounds are produced under iron-limited conditions and play a crucial role in microbial iron acquisition, a vital nutrient for respiration, photosynthesis, and other fundamental processes. Beyond their nutritional function, siderophores also act as plant growth promoters, biocontrol agents, and powerful chelating agents capable of binding a wide range of metal ions. This mechanism is particularly relevant under conditions where metal bioavailability is limited, underscoring the ecological importance of siderophore-mediated uptake [9].

These metabolites have been widely applied in bioremediation due to their ability to solubilize, mobilize, and complex toxic metals and actinides present in soils and industrial wastes, a process governed by metal–ligand affinity and complex stability constants. Several microbial siderophores have demonstrated the capacity to chelate metals under variable pH conditions and mobilize contaminants from mining wastes [10]. Similarly, phytosiderophores exhibit well-defined affinities that enable targeted metal extraction from contaminated soils. This versatility makes siderophores efficient, low-impact tools for sustainable bioremediation strategies [4,11–13].

Despite this remarkable potential, metal-adapted bacteria and their metabolites remain poorly explored as active functional components in engineered biocomposite materials. The incorporation of these microorganisms into composite matrices represents an innovative approach to generating tailor-made biomaterials with enhanced remediation performance. By exploiting their natural metal-binding capacity, it is possible to design bio-based materials with site-specific functionality, offering new opportunities for environmental cleanup technologies.

In this context, this study aimed to isolate indigenous bacterial strains from the Santiago River, select the most promising siderophore-producing microorganism, and immobilize it onto activated carbon to develop a functional carbon-based biocomposite. This strategy proposes an additional remediation alternative to the existing applications of siderophores, integrating biological and physicochemical mechanisms into a single material platform.

On the other hand, biocomposites utilizing carbon-based supports offer significant applications and benefits in the removal of heavy metal ions from contaminated environments. Carbon materials serve as an effective immobilization carrier for microbial cells, enhancing bioremediation through combined adsorption and biological transformation mechanisms [14–16]. These systems leverage the high porosity, extensive surface area, and surface functional groups of activated carbon to adsorb metal ions via electrostatic attraction, ion exchange, and complexation [17,18], while immobilized biomass further reduces metal toxicity through adsorption, accumulation, and metabolite interaction. This synergistic approach improves removal efficiency and sustainability in both aqueous and soil systems [15,19].

In order to evaluate the performance of the proposed biocomposite material, Cu(II) was selected as a model contaminant, which remains one of the most ecotoxicologically relevant metals because of its toxicity at low concentrations and high bioavailability [20]. In this sense, copper has been consistently identified as a persistent contaminant in the Santiago River, reflecting a diverse and sustained industrial activity dating from the 1970s, together with urban pressures [21]. Several studies have shown that Cu preferentially accumulates in river sediments, where concentrations may exceed sediment quality guidelines, indicating a persistent rather than episodic contamination, demonstrating potential ecological risk also present in surface waters, used as a predictor of genotoxicity and cytotoxicity [22–24].

Moreover, copper is described as a traditional model metal ion for assessing the removal performance of several materials [25,26], especially in environmental engineering studies on wastewater and biosorption, due to its prevalence in industrial effluents and its provision of a practical representative target for removal studies [27–29]. Hence, in this work, copper was selected as a probe species to systematically evaluate the adsorption performance of the developed carbon-based biocomposite within the broader context of metal pollution in the Santiago River.

2. Materials and Methods

2.1. Water and Sediment Sampling

Water and sediment samples from the Santiago River riverbank were taken with aseptic containers from two sites (Figure 1). Sterile bottles and sterile plastic bags were used to sample the water and the sediments, using the recommended procedures; three samples were collected at each site (14 October 2024) and averaged to ensure representative results [30].

2.2. Bacteria Isolation and Identification

For bacterial isolation from the sediment samples, 5 g of sediment was aseptically weighed into a sterile container, and 45 mL of 0.9% (*w*/*v*) NaCl Maesa (Mexico city, Mexico) solution, previously sterilized by autoclaving (121 °C, 15 min, 15 psi), was added. The suspension was homogenized under constant agitation for 20 min using a magnetic stir plate inside a laminar flow cabinet. Subsequently, a 1 mL aliquot was transferred to a brand new sterile microtube, and serial tenfold dilutions (10^{-1} to 10^{-10}) were prepared using 0.9% (*w*/*v*) saline solution.

For bacterial isolation from the water sample, 1 mL of the sample was aseptically inoculated into 9 mL of peptone water MCD Lab (Tultitlán, Mexico) sterilized by autoclaving (121 °C, 15 min, 15 psi) and incubated at 35 °C for 18 h. After incubation, serial tenfold dilutions (10^{-1} to 10^{-10}) were prepared in sterile 0.9% (*w*/*v*) saline solution. To verify the sterility of the diluents, a 1 mL aliquot of the sterile saline solution used for the serial dilutions was plated onto Tryptic Soy Agar BD Bioxon (Cuautitlán Izcalli, Mexico) (TSA) plates and incubated at 35 °C for 18 h and used as a sterility control.

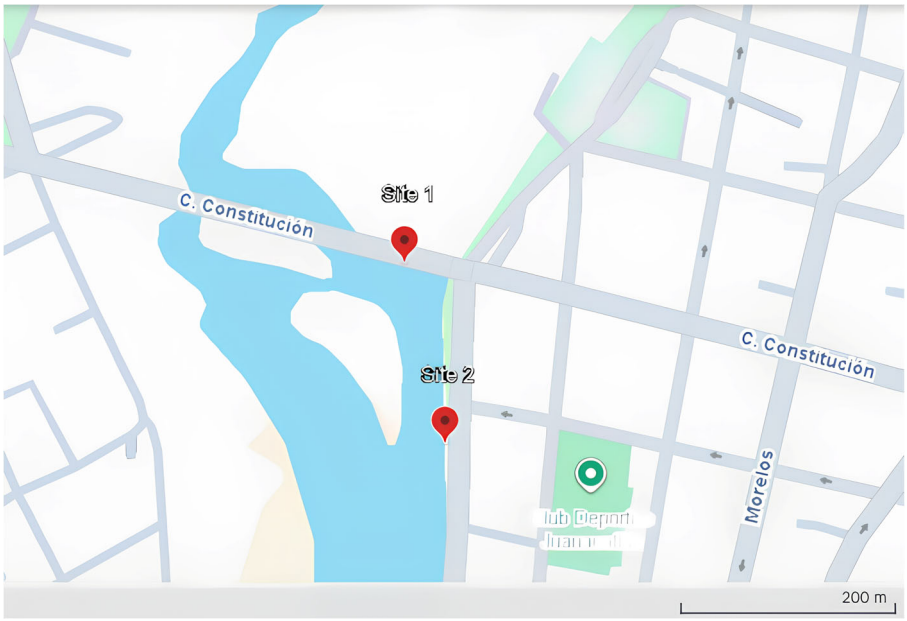

Figure 1. Location of sampling sites of the water and sediment samples near the urban area: 20.512535, −103.173864, site 1, and 20.511049, −103.173507, site 2 (Google Earth).

From each dilution, 100 µL was plated in duplicate onto Tryptic Soy Agar (TSA) plates using the spread plate method and incubated at 35 °C for 18 h. Following incubation, morphologically distinct bacterial colonies were selected and individually transferred to fresh TSA plates by the surface streaking method. The isolated strains were subcultured three to five times under the same incubation conditions to ensure the obtention of pure cultures [31]. Isolates were examined by light microscopy after Gram staining to observe cell morphology and arrangement, Gram response, and culture purity.

For long-term preservation, purified bacterial isolates were cryopreserved in sterile cryovials containing Tryptic Soy Broth (TSB) supplemented with 50% (*v*/*v*) glycerol Sigma-Aldrich (Toluca, Mexico). Prior to cryopreservation, a single well-isolated colony from each bacterial isolate was aseptically transferred into sterile glass vials containing 3 mL of TSB, and the glycerol solution was sterilized by autoclave (121 °C, 15 min, 15 psi) before use. The glass vials were previously washed, disinfected, and sterilized by autoclave (121 °C, 15 min, 15 psi) to ensure aseptic conditions before being filled with the culture media. The inoculated vials were incubated at 36 °C to obtain actively growing cultures. In parallel, one uninoculated vial containing TSB was incubated under the same conditions and used as a sterility control. All cryovials used were brand new to prevent cross-contamination. For each isolated strain, a total of five independent cryovials were prepared to ensure long-term cell availability and experimental reproducibility. The preserved cultures were stored under −80 °C until further use.

For bacterial identification, sample preparation was performed using the Direct Transfer and Extended Direct Transfer methods via MALDI-TOF (Bruker, Bremen, Germany), as indicated by the manufacturer [32], wherein biomass from pure cultures was applied to a stainless-steel target plate. Prior to the MALDI-TOF analysis, an aliquot of each cryopreserved culture selected was retrieved, individually inoculated onto TSA plates, and incubated at 35 °C for 18–24 h to obtain fresh subcultures. To ensure the reliability of the MALDI-TOF identification, from these subcultures, Gram staining and light microscopic observations were performed to evaluate the culture purity. This step served as a critical quality control to verify culture purity and to assess cellular integrity.

Mass spectra were subsequently acquired, and organism identification was achieved by comparing the generated profiles to the BDAL v.12 database via the MALDI BIOTYPER COMPASS platform (Bruker, Bremen, Germany). Only fresh subcultures were used for biomass harvesting, as this optimal growth phase provides consistent protein profiles essential for accurate spectral analysis.

All microbiological procedures, including sample collection and handling, dilution preparation, plating, and isolate manipulation, were conducted under a laminar flow cabinet to ensure aseptic conditions and operator safety. All biological waste generated during the experimental procedures, including culture media, disposable materials, and contaminated consumables, was handled and disposed of in accordance with institutional biosafety protocols for biological hazardous waste.

2.3. CAS Reagent (Solid and Liquid Media)

For the preparation of 1 L of the colorimetric ternary complex, three separate stock solutions were prepared as follows: (i) 0.06 g of Chrome Azurol S (CAS) Sigma-Aldrich (St. Louis, MO, USA) was dissolved in 50 mL of double-distilled water (ddH_2O); (ii) 0.073 g of hexadecyltrimethylammonium bromide (HDTMA) Sigma-Aldrich (Shanghai, China) was dissolved in 40 mL of ddH_2O; and (iii) individual solutions of chloride salts (1.66 mM) for each of the selected metal cations ($FeCl_3 \cdot 7H_2O$, $CuCl_2$, $CoCl_2$, $ZnCl_2$, and $NiCl_2$) Sigma-Aldrich (Darmstadt, Germany) were dissolved in 10 mM HCl Golden Bell (Mexico City, Mexico). The stock solutions were sterilized by autoclaving at 121 °C for 15 min at 15 psi. Subsequently, under sterile conditions, 50 mL of the CAS solution, 40 mL of the HDTMA solution, and 9 mL of the corresponding metal cation solution were combined and brought to a final volume of 100 mL with ddH_2O.

For the base medium, three independent base solutions were prepared as follows: (i) 0.1 g of $MgSO_4 \cdot 7H_2O$ was dissolved in 20 mL of ddH_2O; (ii) 0.45 g of K_2HPO_4 was dissolved in 20 mL of ddH_2O; and (iii) 0.1 g of KCl was dissolved in 20 mL of ddH_2O. The three solutions were combined, and 0.2 g of yeast extract and 750 mL of ddH_2O were added. The pH of the base medium was adjusted to 5.6 using HCl. It was then supplemented with 15 g of bacteriological agar MCD Lab (Tultitlán, Mexico), and 60 mL of ddH_2O was added. The base medium was sterilized by autoclaving (121 °C, 15 min, 15 psi).

Once the base medium had cooled to approximately 50–55 °C, the following sterile components were aseptically incorporated: 10 mL of 1M NH_4Cl Fermont (Monterrey, Mexico) (autoclave-sterilized), 20 mL of 20% *w*/*v* glucose (filter-sterilized through a 0.22 µm membrane), and 100 mL of the corresponding CAS-HDTMA-metal complex. The mixture was kept under agitation to ensure homogeneous distribution of the components.

The liquid assay was prepared as described in [33] without modifications. Briefly, the CAS reagent was prepared by mixing solutions of Chrome Azurol S, iron (III) chloride, and the quaternary ammonium detergent hexadecyltrimethylammonium bromide (HDTMA) in a piperazine buffer to form a stable blue complex. Cell-free culture supernatants (or test solutions) were then added to the CAS reagent in a 1:1 ratio, mixed, and incubated at 37 °C. The removal of iron from the blue CAS dye complex by a stronger chelator causes a colorimetric shift from blue to orange/yellow.

2.4. Computer-Assisted Metallophore Quantification

For image analysis, MATLAB 2025a (The MathWorks, Natick, MA, USA) was used to develop a script to meet the specific needs of this investigation. To enable the quantitative characterization of siderophore production, image normalization was performed [34,35]. The script utilizes the HSV (Hue, Saturation, Value) color space, which offers significant advantages over the RGB model for computer vision applications. The HSV model de-

composes visual information into three intuitive components: Hue (defining the dominant wavelength of the color), Saturation (quantifying color purity), and Value (determining light intensity). This decomposition ensures precise color identification and segmentation based on tonal signature, providing robustness against shadows, reflections, and exposure variation, a critical feature for accurately detecting areas where color shifts indicate the presence of metallophores in the CAS assays [36]. Most analyses consider only a positive result to the assay, while in this contribution, the colored area is divided into two intensity levels, as seen in Figure 2. The effective area is defined as $A_T = A_{high} + \frac{1}{2}A_{intermediate}$, where the intensities are defined by the user according to the initial color of the medium.

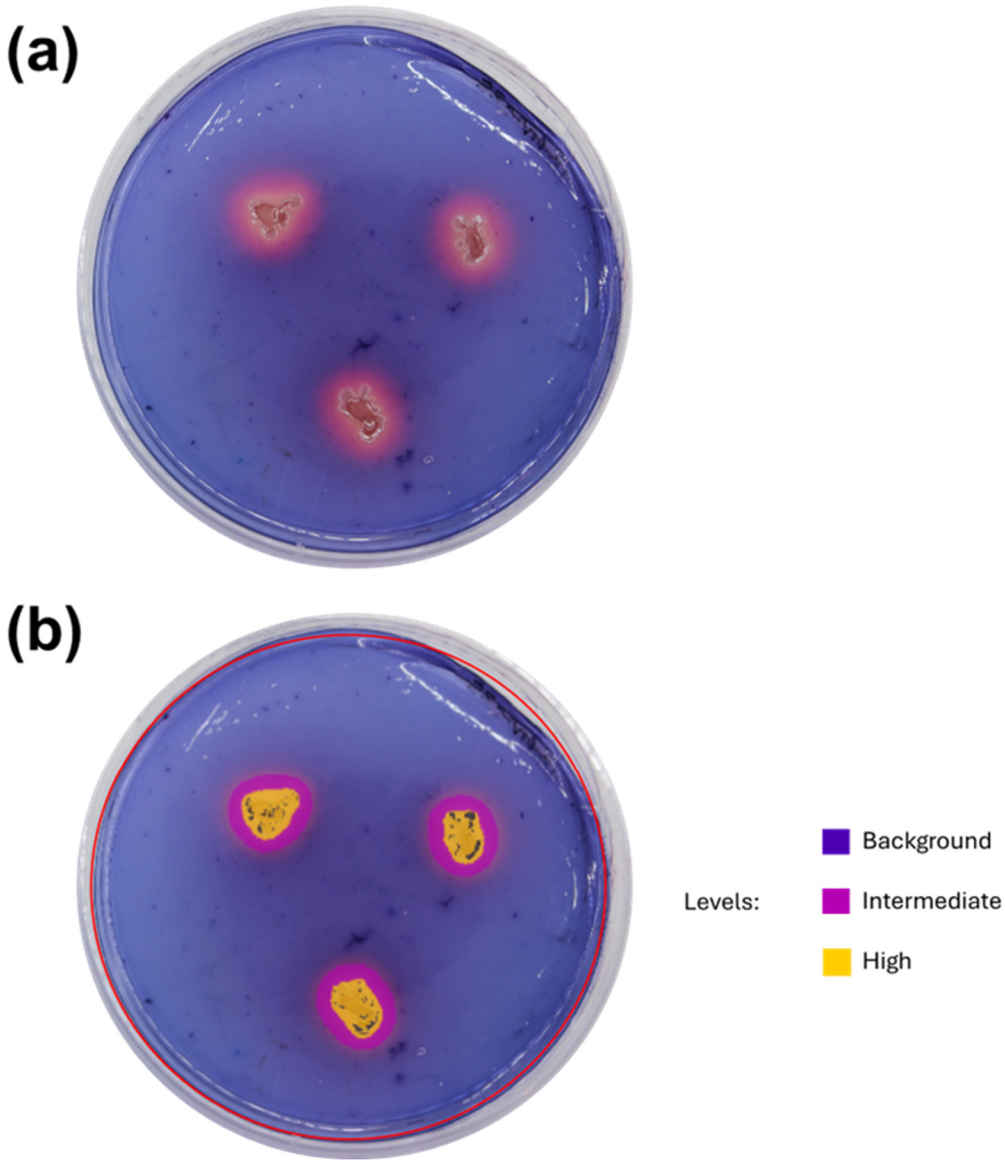

Figure 2. Illustration of the MATLAB image analysis usage. (**a**) A picture of a Petri dish with *Escherichia coli* colonies from a water sample of sampling site 1 with the modified CAS medium containing Cu(II). (**b**) The MATLAB script lets the user define the area of the Petri dish (90 mm diameter); then, according to the color intensity, it identifies the positive metallophore activity of the bacteria and classifies it into two intensities, intermediate and high.

2.5. Development of Carbon-Based Biocomposite (CBM)

Bacillus thuringiensis was cultured at 37 °C in Tryptic Soy Broth (TSB) medium (Difco Lab) at pH 7 [16]. This bacteria suspension was centrifuged and washed twice with sterile

distilled water; then, it was re-dispersed in 20 mL of this water. This suspension was used as a blank.

The adsorption experiments on the samples used 0.15 g of activated carbon C (Mega, Carbotecnia, Zapopan, Mexico) as a support material for the biocomposite. This carbon corresponds to a granular activated carbon of vegetal origin (pine wood), chemically activated with phosphoric acid, characterized by a predominantly meso- and microporous structure. The textural characterization of the activated carbon was carried out by N_2 adsorption at −196 °C using Micromeritics TriStar II PLUS equipment (Micromeritics Instruments Corporation, Norcross, GA, USA). The material exhibits an S_{BET} (756 $m^2\ g^{-1}$), L_0 (2.17 nm), W_o (0.401 $cm^3\ g^{-1}$), $V_{0.95}$ (0.779 $cm^3\ g^{-1}$), and V_{meso} (0.3780 $cm^3\ g^{-1}$), indicating a highly effective surface area, suitable for microbial immobilization and biocomposite formation. Additional properties include an apparent density of 0.23 g cm^{-3} and a particle size distribution of 14 × 35 mesh.

The activated carbon was suspended in 5 mL of the bacterial suspension, which was stirred with a vortex mixer and then maintained in an orbital shaker (room temperature, 45 RPM), CBM. The steady state was reached after 300 min. Although other microorganisms reported a higher siderophore production, our choice relies on its safety for laboratory tests, since this microorganism is classified as such in several standards, having several commercial applications [37]. All tests were performed in closed laboratory conditions.

2.5.1. Physicochemical Characterization of Carbon Materials (C and CBM)

The morphology of carbon materials was examined by scanning electron microscopy (SEM) and energy dispersive spectroscopy (EDX). The SEM micrographs and EDX spectra were obtained using a scanning electron microscope JSM IT710HR JEOL (Tokyo, Japan).

Fourier-transform infrared spectroscopy (ATR-FTIR) studies were performed to study the chemical surface modification due to the introduced biomass to be supported onto activated carbon. For this purpose, a Nicolet iS5 FTIR Thermo Scientific (Madison, WI, USA) spectrometer equipped with a diamond-tipped attenuated total reflectance (ATR) device was used. The spectra of all samples correspond to 32 scans with resolutions of 0.8 cm^{-1} and a data spacing of 0.060 cm^{-1}.

2.5.2. Cu(II) Adsorption Experiments in Aqueous Solution

Adsorption of Cu(II) in an aqueous solution was studied for the prepared carbon materials. Cu(II) solutions were prepared using $CuSO_4 \cdot 5H_2O$ Sigma-Aldrich (Madrid, Spain) solutions in distilled water at different concentrations. The experiments were carried out employing 0.4 g of adsorbent in 40 mL of the Cu(II) solution and were mechanically agitated at 180 rpm at ambient temperature. The concentration of Cu(II) in the solution was determined by UV–Vis spectroscopy through the formation of an intense blue ammonia copper complex at a maximum wavelength of 611 nm using the spectrophotometer UV-2600i Shimadzu (Kyoto, Japan). All experiments were carried out in duplicate. The adsorption capacity of the materials was calculated from a mass balance.

To investigate the effect of time in the adsorption process, kinetic models were used to test the experimental data [38]. Briefly, the pseudo-first-order equation of Lagergren is expressed as Equation (1):

$$q_t = q_e\left(1 - e^{-k_1 t}\right) \quad (1)$$

where q_e (mg g^{-1}) and q_t (mg g^{-1}) are the amounts of adsorbed adsorbate at equilibrium and at time t, respectively, and k_1 (min^{-1}) is the rate constant of pseudo-first-order adsorp-

tion. If the rate of adsorption has a second-order mechanism, the pseudo-second-order chemisorption kinetic rate equation can be expressed as Equation (2):

$$q_t = \frac{t}{\frac{1}{k_2 q_e^2} + \frac{t}{q_e}} \quad (2)$$

where k_2 (g mg^{-1} min^{-1}) is the equilibrium rate constant of pseudo-second-order adsorption.

The experimental equilibrium data were modeled using Langmuir and Freundlich models [38]. According to the Langmuir isotherm model, the adsorption process occurs at specific homogeneous sites on the adsorbent surface until a complete monolayer is formed. This model is used to estimate the maximum adsorption capacity that corresponds to the adsorbent saturation. The Langmuir model is mathematically represented as Equation (3):

$$q_e = \frac{q_{max} K C_e}{1 + K C_e} \quad (3)$$

where q_{max} (mg L^{-1}) is the maximum adsorption capacity of the adsorbent, K (mg^{-1} L) is the Langmuir constant indicating affinity for the active site and is related to the heat of adsorption, and C_e (mg L^{-1}) is the concentration of the analyte in equilibrium conditions. On the other hand, the Freundlich model can be used to describe the adsorption on a heterogeneous surface or a surface supporting different sites and is not, therefore, restricted to the formation of a monolayer. The Freundlich model is mathematically represented as Equation (4):

$$q_e = K_f {C_e}^{1/n} \quad (4)$$

where K_f (mg^{n} L^{-n}) is the Freundlich constant, and $1/n$ is the heterogeneity factor.

Finally, to evaluate the potential use of the CBM as an adsorbent material, the toxicity of the treated effluents was determined by the measurement of the inhibition of the bacteria *Vibrio fischeri*, Strain Passport: NRRL-B-11177, in accordance with the European guideline ISO 11348-2:2007 [16].

2.5.3. Mathematical Analysis for Data Fitting

Prior to the analysis, all FTIR spectra were pre-processed using OriginPro (OriginLab Corporation, Northampton, MA, USA). Baseline correction was applied to eliminate background contributions, followed by spectral smoothing using the adjacent-averaging method to reduce experimental noise. Subsequently, the spectra were mathematically treated and converted to transmittance units for proper visualization and interpretation of the absorption bands. Each sample was analyzed in triplicate (n = 3) to ensure reproducibility. The resulting spectra showed high consistency among repetitions; therefore, a representative spectrum is presented. The variability between replicates was evaluated by calculating the standard deviation of peak intensities, which remained below 5% for the main absorption bands, indicating good experimental repeatability.

For SEM-EDX measurements, the value of n corresponds to five independent particles of the CBM material. Each particle was analyzed and mapped in at least three different zones to account for surface heterogeneity. The spectra shown in each figure correspond to the specific points (Spc) indicated directly on the SEM micrographs. Although multiple particles and regions were evaluated, the elemental composition and trends were highly consistent across all measurements. Therefore, the figures presented in the manuscript correspond to representative images, as similar results were obtained in all cases.

All adsorption experiments were conducted in duplicate (n = 2) under identical conditions. The results are reported as mean values ± standard deviation. Error bars were

included in the kinetic and isotherm plots to reflect experimental variability. The kinetic and equilibrium models were fitted by adjusting the experimental data to the corresponding non-linear equations using the Levenberg–Marquardt algorithm implemented in STATISTICA 7.0 (TIBCO, San Ramon, CA, USA). Model performance was evaluated using the coefficient of determination (R).

3. Results and Discussion

3.1. Water and Sediment Analysis

The water samples were analyzed using an ELAN 9000 (PerkinElmer, Shelton, CT, USA) following the EPA 6010B/NMX-AA-051-SCFI-2016 method for water samples and the EPA 3050 method for metals in the sediment samples. The water and sediment analysis results, as shown in Table 1, agree with those found on the Water Commission of Jalisco website (refer to data availability at the end of this document for the link). In the water samples, Mg and Zn are not specified in the Mexican norm [39], and the metals of concern are below the norm. On the other hand, in the Mexican norm [40] on contaminated soil does not consider Fe, Cu, Zn, or Mg. The analyzed metals of concern, such as Cr, Cd, or Ni, are below the specified limits for agricultural, housing, commercial, or industrial uses. Based on the water quality monitoring data, the Santiago River contains low levels of various heavy metals, which are below the maximum permissible limits set by Mexican norms. However, significant exceptions may occur, which may be correlated to the rainy season, as seen in Appendix A (Figure A1), due to transfer from the sediments to the water stream. Studies have recorded sporadic but significant contamination events. As expected, the sediment samples reveal a high concentration of metals; nonetheless, these concentrations are close but below the threshold values specified in the Mexican official standards of soil for agriculture.

Table 1. Water and sediment analysis of several metal cations via ICP.

Cation	Site 1		Site 2	
	Water (mg L^{-1})	**Sediment (mg kg^{-1})**	**Water (mg L^{-1})**	**Sediment (mg kg^{-1})**
Fe^{2+}	0.07	25,150.00	0.03	18,800.00
Cu^{2+}	<0.01	110.00	<0.01	28.87
Cr^{2+}	<0.01	241.50	<0.01	18.35
Cd^{2+}	<0.01	4.70	<0.01	<0.25
Ni^{2+}	<0.01	48.25	<0.01	10.50
Zn^{2+}	<0.01	469.90	<0.01	38.00
Mg^{2+}	28.92	3201.00	29.5	3132.00

3.2. Bacteria Identification

The analysis demonstrated successful taxonomic identification of the cultures of interest. Table 2 summarizes the resulting taxonomic assignments along with their respective sample sites via MALDI-TOF; only scores above 1.70 are considered a high match [41]. Furthermore, the table compiles the existing literature on siderophore production by these taxa, some of which provide quantitative measurements via the CAS liquid assay.

Table 2. Taxonomic identification and reported siderophore production (NA = not available or qualitative report).

ID *	Microorganism	Reported Siderophore Production
W1-01	*Enterobacter bugandensis*	~60%, [42]
W1-01	*Escherichia coli*	~75%, [43]
W1-03	*Bacillus subtilis*	NA, [44]
W1-04	*Pseudomonas oleovorans*	NA, [45]
W1-05	*Pseudomonas mendocina*	NA, [46]
W1-06	*Citrobacter freundii*	100%, [47]
W1-07	*Citrobacter koseri*	~76%, [47]
W1-08	*Acinetobacter tandoii*	NA, [48]
W2-01	*Bacillus velezensis*	NA, [49]
W2-02	*Enterobacter hormaechei*	NA, [50]
W2-03	*Pseudomonas otitidis*	NA, [51]
W2-04	*Morganella morganii*	NA, [52]
W2-05	*Klebsiella pneumoniae*	NA, [53]
W2-06	*Bacillus thuringiensis*	NA, [54]
S1-01	*Priestia megaterium*	~78%, [55]
S2-01	*Bacillus mojavensis*	NA, [56]
S2-02	*Bacillus altitudinis*	NA, [57]
S2-03	*Citrobacter freundii*	NA, [58]
S2-04	*Bacillus pumilus*	NA, [59]
S2-05	*Bacillus licheniformis*	NA, [60]

* The ID is coded as follows: W stands for water; S stands for soil; 1, 2 are the sampling sites described above; and -0X is an identification number.

A total of 192 bacterial isolates were obtained, of which 74 were positive for siderophore production on CAS medium. Based on the highest quantitative siderophore production levels observed during initial screening, a representative subset of isolates was selected for taxonomic identification via MALDI-TOF to maximize the resource allocation toward the most potent producers. In Table 3, bacteria with the highest siderophore production are shown, both with the MATLAB image analysis and the liquid CAS assay, as described in [33], where the siderophore percentage is computed as Equation (5):

$$\%SU = \frac{A_r - A_s}{A_r} \times 100 \quad (5)$$

Table 3. Overall siderophore-producing bacteria along with *Bacillus thuringiensis*, the benchmark microorganism of the biocomposite.

Microorganism	Overall Dish Area per Colony (mm^2)	Liquid CAS Assay (%SU)	Affinity Order
Enterobacter bugandensis	173.60	0	Cu, Ni, Zn, Fe, Co
Priestia megaterium	129.79	74.24	Ni, Cu, Co, Fe, Zn
Enterobacter hormaechei	72.31	15.47	Ni, Zn, Cu, Co, Fe
Citrobacter koseri	84.45	32.61	Ni, Zn, Fe, Cu, Co
Escherichia coli	111.47	17.52	Zn, Ni, Fe, Co, Cu
Acinetobacter tandoii	34.33	73.29	Ni, Fe, Co, Zn, Cu
Bacillus thuringiensis	93.13	47.17	Ni, Fe, Zn, Cu, Co

* The ID is coded as follows: W stands for water; S stands for soil; 1, 2 are the sampling sites described above; and -0X is an identification number.

3.3. Development of Biocomposite Materials Useful for the Remediation of Contaminated Effluents: Proof-of-Concept Studies

Figure 3 shows the physicochemical characterization of the studied carbon materials. SEM micrographs revealed morphological differences between the surface of the C and the CBM. The C displayed a porous surface, with well-defined channels and an average diameter of 10 µm, typical of activated carbons [18] (Figure 3a). In contrast, the CBM showed an extensive, homogeneous covering over the porous texture of the carbon, attributable to the immobilized biomass, confirming the successful formation of a biomass layer on the support material [14] (Figure 3b). Elemental analysis via SEM-EDX of the CBM revealed the presence of phosphorus (Figure A2), a constituent element of bacterial biomolecules [17] that was not present in the C, corroborating the presence of biomass and providing evidence of potentially metal-coordinating functional groups.

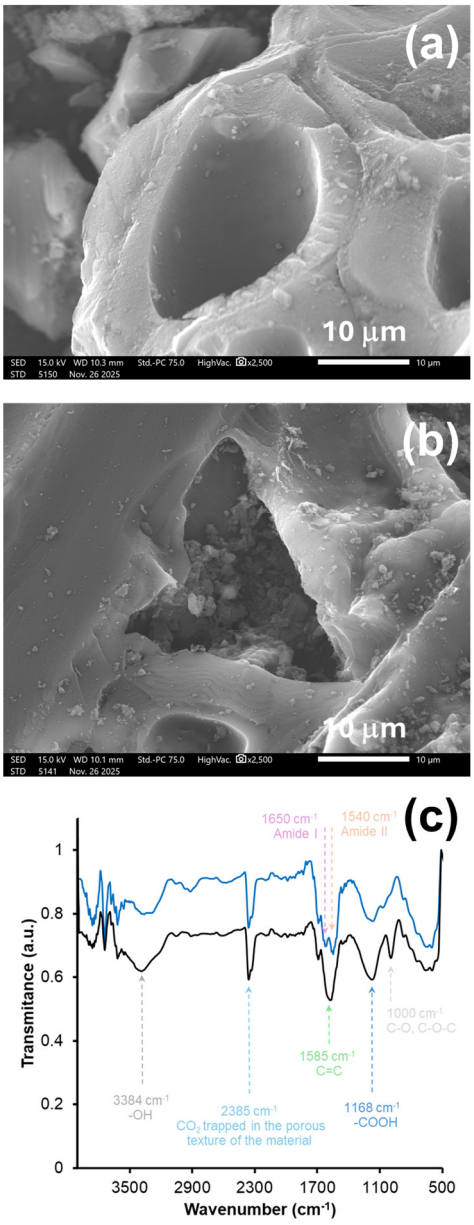

Figure 3. Physicochemical characterization via SEM (**a**, sample C; **b**, sample CMB) and (**c**) ATR-FTIR of C (activated carbon, black) and biocomposite CMB (blue).

Regarding surface chemistry, ATR-FTIR spectroscopy studies show characteristic bands of oxygenated groups, mainly -OH, C-O, and C-O-C, centered approximately at 3600,

1585, and 1000 cm^{-1} (Figure 3c, black) [17]. After the biomass incorporation, the material exhibits changes in surface chemistry. In the ATR-FTIR spectrum of the CBM (Figure 3c, blue), an attenuation of the band at ~1000 cm^{-1}, assigned to C–O/C–O–C stretching of surface oxygenated groups, is observed, suggesting that these groups participate in the initial attachment of the biomass to the activated carbon, acting as anchoring sites. Significant changes are highlighted in the region near 1600 cm^{-1}. The FTIR spectrum of the untreated activated carbon surface shows a main band near 1585 cm^{-1}, attributed to C=C modes of the carbonaceous structure. After the biomass incorporation to the carbon, this signal resolved into two clearly defined bands: ~1650 cm^{-1} (Amide I) and ~1540 cm^{-1} (Amide II) [61], attributable to characteristic vibrations of peptide bonds. These spectral changes indicate the adsorption/accumulation of proteins in the activated carbon support.

To evaluate the adsorption capacity of the CBM for Cu(II) present in the aqueous solution, adsorption experiments were conducted using carbonaceous materials. Kinetic studies show a characteristic profile for both cases, with an initial rapid phase followed by equilibrium (Figure 4a), attributable to the metal binding to readily available surface-active sites. Fitting to adsorption kinetic models (Table 4) shows that the rate for CBM is much slower than for C (0.02 min^{-1} vs. 0.14 min^{-1}), suggesting that the initial process rate is predominantly governed by metal diffusion toward the carbon surface and that the immobilized biomass layer represents a diffusional barrier for its adsorption. This is possibly because colonization occurred mainly within the meso- and macroporosity of the support. However, equilibrium is reached after 60 min, demonstrating an increase in adsorption capacity attributable to the presence of the biomass.

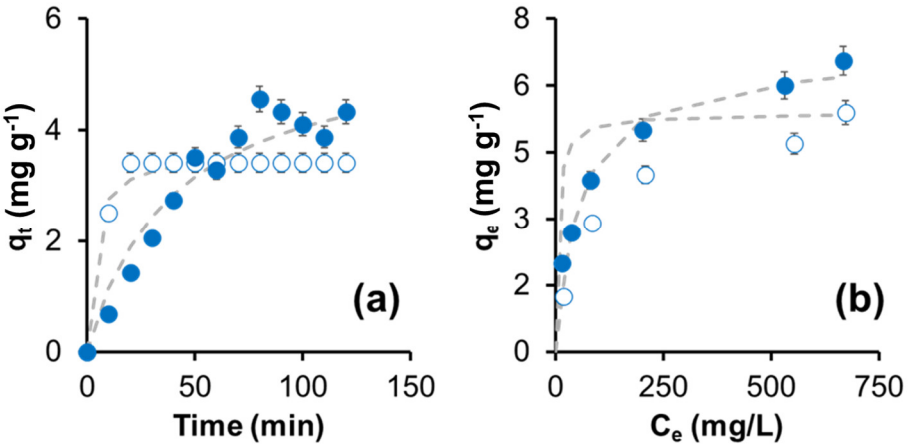

Figure 4. Adsorption studies of (**a**) adsorption kinetics (pseudo-first-order fit) and (**b**) adsorption equilibrium of Cu(II) (Langmuir fit) onto ○ C and ● CBM.

Table 4. Kinetic and equilibrium constants for the proposed models used to study the adsorption capacity of Cu(II) on C and CBM.

Materials	Pseudo-First-Order			Pseudo-Second-Order			Langmuir			Freundlich		
	q_e (mg g^{-1})	k_1 (min^{-1})	R	q_e (mg g^{-1})	k_2 (g mg^{-1} min^{-1})	R	q_{max} (mg g^{-1})	K	R	K_f	n	R
C	3.43	0.14	0.99	3.58	0.06	0.88	5.38	0.18	0.98	0.77	3.39	0.98
CBM	4.42	0.02	0.99	5.67	0.21	0.88	6.67	0.01	0.99	1.03	3.50	0.99

On the other hand, the adsorption equilibrium studies (Figure 4b) showed a significant difference between the two materials. The maximum adsorption capacity calculated according to the Langmuir isotherm model for CBM was 6.67 mg/g, while for C, it was 5.38 mg/g (Table 4). This 23.9% increase in the adsorption capacity of the biomass-containing material

indicates that, at equilibrium, the immobilized biomass contributes additional adsorption sites for metal retention, which adds to the intrinsic capacity of the carbon. Figure A3 presents SEM-EDX mapping of the CBM, demonstrating the accumulation of the metal after the adsorption process.

Finally, to evaluate the final toxicity of the treated effluent, bioassays were performed with solutions containing the same final Cu(II) concentration (5 ppm). This was done to isolate the effect of metal speciation (its chemical form and bioavailability) from the effect of its total concentration. Under this condition, the C effluent showed a 38.6% inhibition of *V. fischeri* luminescence. In contrast, the CBM effluent showed a significantly lower inhibition (29.6%). Based on this, it is proposed that the CBM not only adsorbs the metal but also modifies its speciation and bioavailability. The significant reduction in acute toxicity indicates that the immobilized biomass is not simply retaining Cu(II) physically but is immobilizing it through more stable chemical mechanisms, including possible chelation by siderophores and coordination with other functional groups in the extracellular matrix.

The obtained results position CBM not as a simple adsorbent with incremental capacity but as a conceptual proposal for a hybrid material with enhanced function. While C operates primarily through physical adsorption mechanisms that can be reversible, CBM introduces a chemical immobilization mechanism that generates an effluent with a lower inherent ecotoxicological risk. Therefore, the value of this immobilization strategy lies in its potential to develop remediation processes that are not only more efficient in terms of capacity but also intrinsically safer for receiving ecosystems by mitigating the residual toxicity of the treated water. This work establishes a solid proof of concept for this proposal, highlighting the importance of assessing toxicity as a critical parameter in the design of new remediation materials.

4. Conclusions

The bacteria found in the water and sediment samples of the Santiago River in Jalisco, Mexico, have been exposed to several metal ions, particularly in the sediments. Although most of the metals are below the permitted threshold according to Mexican regulations, the soil can release metals by desorption processes, and accumulation in living beings is known to happen. The river has a "self-regulation" mechanism through the bacteria found in the water and the sediments whose metabolites (siderophores or others) can reduce the toxicity of the metals by themselves. Also, many of these bacteria are known to have interactions with the rhizosphere, thus enhancing the metal removal by phytoremediation. In this sense, the bacteria isolates can be further studied to find the optimal siderophore production to promote remediation processes.

This research work demonstrates that bacteria isolated from the Santiago River are not only a valuable resource due to their siderophore production but also a key component for engineering advanced remediation materials. The successful engineering of a carbon-based biocomposite (CBM) through the immobilization of *Bacillus thuringiensis* biomass onto activated carbon translates this natural capacity into a functional hybrid system. The CBM not only exhibited a higher Cu(II) adsorption capacity compared to pristine carbon, but, more importantly, it significantly reduced the residual toxicity of the treated effluent. This highlights the following key advancement: the biocomposite shifts the removal mechanism from reversible physical adsorption toward more stable chemical immobilization, likely mediated by siderophore chelation, thereby altering the metal's speciation and bioavailability. This proof of concept positions CBM as a strategic material that offers the dual advantage of enhanced efficiency and a safer output, representing a critical step in developing remediation technologies that protect ecosystem health beyond mere contaminant concentration reduction.

Author Contributions: Conceptualization, M.A.Z.-N., M.R.C.-R., and F.P.-A.; methodology, M.A.Z.-N., F.P.-A., N.N.G.-V., L.A.R.-C., M.I.B.-T., F.C.-M., and M.R.C.-R.; software, M.A.Z.-N. and M.R.C.-R.; validation, K.S.-G. and C.S.G.-N.; formal analysis, K.S.-G. and N.N.G.-V.; investigation, M.A.Z.-N., N.N.G.-V., M.R.C.-R., C.S.G.-N., and F.P.-A.; resources, M.A.Z.-N., N.N.G.-V., F.P.-A., and K.S.-G.; data curation, M.A.Z.-N., L.A.R.-C., M.I.B.-T., F.C.-M., and F.P.-A.; writing—original draft preparation, M.A.Z.-N., F.P.-A., and M.R.C.-R.; writing—review and editing, N.N.G.-V., L.A.R.-C., and K.S.-G.; visualization, M.A.Z.-N. and L.A.R.-C.; supervision, M.A.Z.-N. and F.P.-A.; project administration, M.A.Z.-N. and M.R.C.-R.; funding acquisition, M.A.Z.-N., N.N.G.-V., F.P.-A., and K.S.-G. All authors have read and agreed to the published version of the manuscript.

Funding: This research was funded by SICYT-COECyTJAL, grant number FODECIJAL-11178, and co-funded by the *Fondo Semilla—Decanato de Diseño, Ciencia y Tecnología* from *Universidad Autónoma de Guadalajara* as part of the project agreement.

Institutional Review Board Statement: Not applicable.

Informed Consent Statement: Not applicable.

Data Availability Statement: Data are contained within the article. Water quality assessments of Jalisco's most important watersheds can be found at (Spanish) https://www.ceajalisco.gob.mx/contenido/datos_abiertos/, accessed on 5 July 2025.

Acknowledgments: M.R.C.-R. thanks the *Universidad Autónoma de Guadalajara* for the scholarship received for the completion of undergraduate studies. C.S.G.-N. expresses her gratitude to Francisco Carrasco-Marín and the UGR-Carbon group at Universidad de Granada for hosting a research stay that enabled carrying out a fundamental part of the research work. The authors acknowledge Lydia Olvera from CIDI-UAG for granting access to the analytical equipment and Sofía Jaime-Vargas and Esthefanya Rangel-Domínguez for their valuable support in the laboratory experiments.

Conflicts of Interest: The authors declare no conflicts of interest.

Appendix A

Supplementary information is contained in this Appendix.

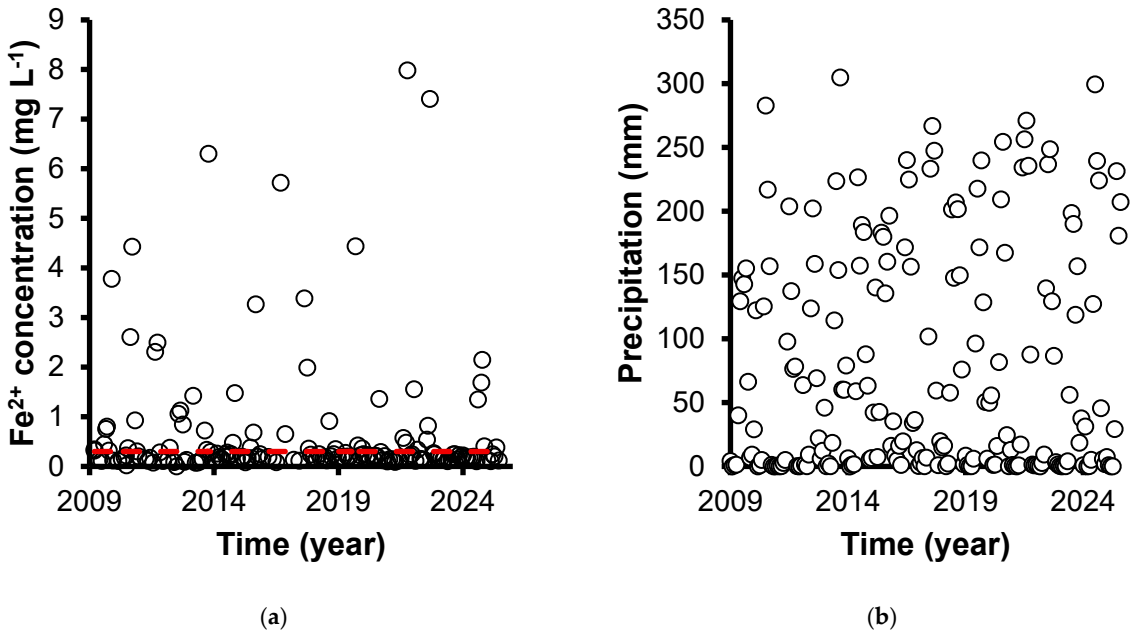

(**a**) (**b**)

Figure A1. (**a**) Historical data from the Comisión Estatal del Agua for iron. The red line denotes the iron threshold according to the Mexican regulations NOM-127-SSA1-2021; (**b**) however, this is not necessarily correlated with discharges but probably with the transfer from the sediments to the river stream during the rainy season.

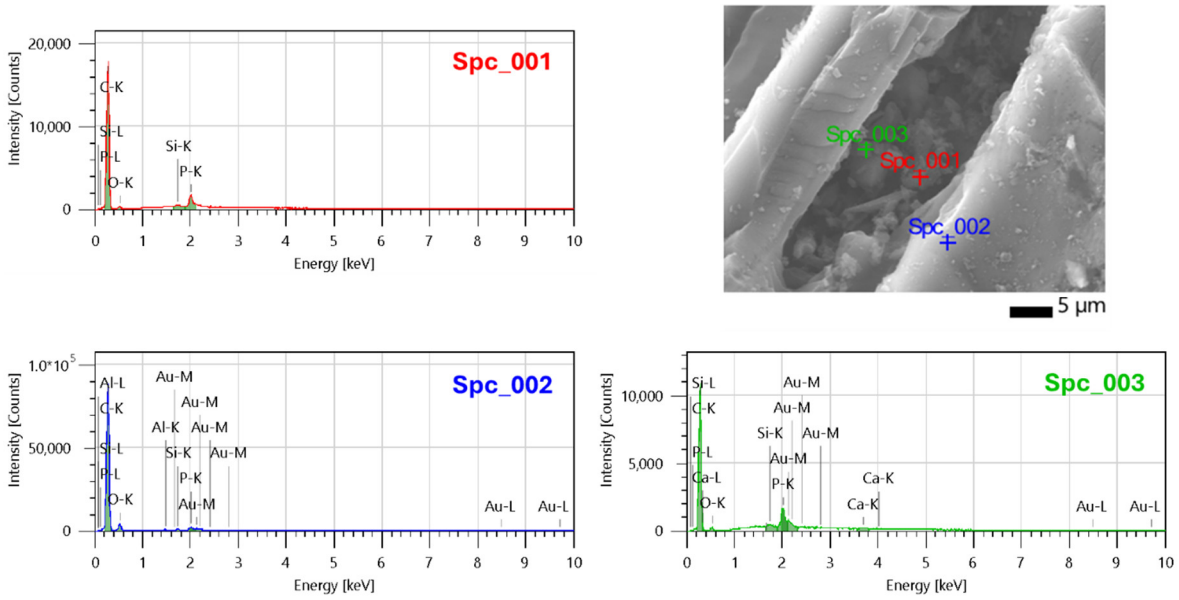

Figure A2. Semi-quantitative assessment of the CBM surface prior to adsorption studies. SEM micrograph showing three different sampling zones (Spc_001–Spc_003) analyzed by EDX. The corresponding spectra are displayed for each selected point. The analysis was performed on n = 5 independent particles, each mapped in at least three different regions. The image shown is representative, as similar elemental distributions were observed for all analyzed particles.

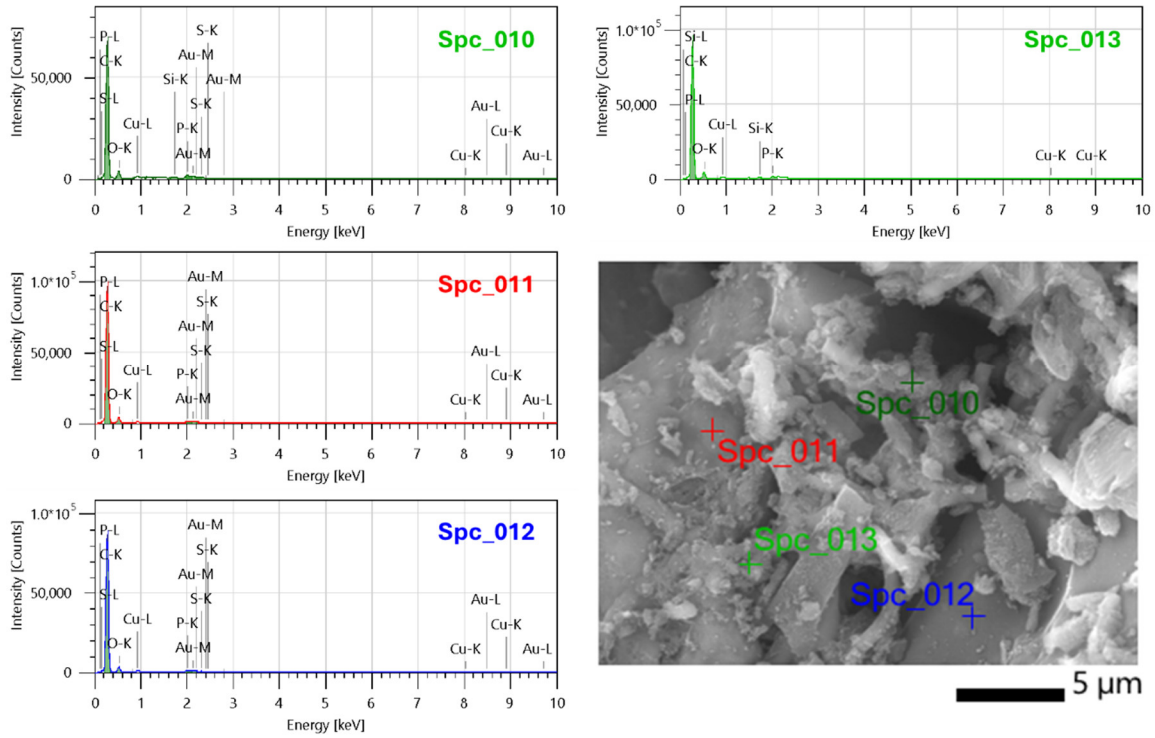

Figure A3. Semi-quantitative evaluation of Cu(II) adsorption on CBM. SEM micrograph showing four different sampling zones (Spc_1–Spc_4) analyzed by EDX after Cu(II) adsorption. The corresponding spectra are displayed for each indicated point. The analysis was conducted on n = 5 independent particles, each mapped in at least three different regions. The image shown is representative of the material, since consistent results were obtained across all analyzed particles.

Table A1. Details on the positive area of the selected microorganisms with the highest color change.

Microorganism	Area (mm^2)				
	Fe	Co	Zn	Ni	Cu
Enterobacter bugandensis	51.52	39.66	242.27	186.76	347.84
Priestia megaterium	14.85	43.50	9.10	356.51	224.99
Enterobacter hormaechei	17.21	26.67	117.48	131.38	68.82
Citrobacter koseri	58.23	26.44	80.96	223.25	33.35
Escherichia coli	133.63	103.23	164.66	136.34	19.48
Acinetobacter tandoii	30.45	30.26	24.89	78.32	7.73
Bacillus thuringiensis	64.52	21.07	51.81	307.03	21.22

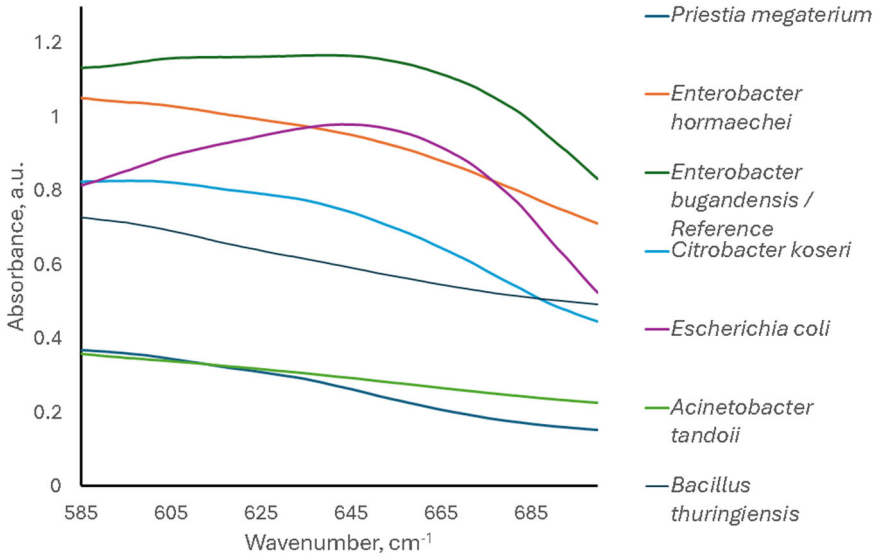

Figure A4. Absorbance scan of the liquid CAS assay. The absorbance at a wavenumber of 630 cm^{-1} was used to compute the siderophore percentage.

References

1. Núñez-Razo, I.; de Anda, J.; Barrios-Piña, H.; Olvera-Vargas, L.A.; García-Ruíz-García, M.; Hernández-Morales, S. Development of a Watershed Sustainability Index for the Santiago River Basin, Mexico. *Sustainability* **2023**, *15*, 8428. [CrossRef]
2. Rizo-Decelis, L.D.; Andreo, B. Water Quality Assessment of the Santiago River and Attenuation Capacity of Pollutants Downstream Guadalajara City, Mexico. *River Res. Appl.* **2016**, *32*, 1505–1516. [CrossRef]
3. Hesse, E.; O'Brien, S.; Tromas, N.; Bayer, F.; Luján, A.M.; van Veen, E.M.; Hodgson, D.J.; Buckling, A. Ecological Selection of Siderophore-Producing Microbial Taxa in Response to Heavy Metal Contamination. *Ecol. Lett.* **2018**, *21*, 117–127. [CrossRef] [PubMed]
4. Arroyo-Herrera, I.; Román-Ponce, B.; Reséndiz-Martínez, A.L.; Estrada-de los Santos, P.; Wang, E.T.; Vásquez-Murrieta, M.S. Heavy-Metal Resistance Mechanisms Developed by Bacteria from Lerma–Chapala Basin. *Arch. Microbiol.* **2021**, *203*, 1807–1823. [CrossRef]
5. Złoch, M.; Thiem, D.; Gadzała-Kopciuch, R.; Hrynkiewicz, K. Synthesis of Siderophores by Plant-Associated Metallotolerant Bacteria under Exposure to Cd^{2+}. *Chemosphere* **2016**, *156*, 312–325. [CrossRef]
6. Wang, Y.; Huang, W.; Ali, S.W.; Li, Y.; Yu, F.; Deng, H. Isolation, Identification, and Characterization of an Efficient Siderophore Producing Bacterium from Heavy Metal Contaminated Soil. *Curr. Microbiol.* **2022**, *79*, 227. [CrossRef]
7. Mitra, A.; Chatterjee, S.; Kataki, S.; Rastogi, R.P.; Gupta, D.K. Bacterial Tolerance Strategies against Lead Toxicity and Their Relevance in Bioremediation Application. *Environ. Sci. Pollut. Res.* **2021**, *28*, 14271–14284. [CrossRef]
8. Schalk, I.J.; Hannauer, M.; Braud, A. New Roles for Bacterial Siderophores in Metal Transport and Tolerance. *Environ. Microbiol.* **2011**, *13*, 2844–2854. [CrossRef]
9. Senthilkumar, M.; Amaresan, N.; Sankaranarayanan, A. *Plant-Microbe Interactions*; Humana Press: New York, NY, USA, 2021. [CrossRef]
10. Ahmed, E.; Holmström, S.J.M. Siderophores in Environmental Research: Roles and Applications. *Microb. Biotechnol.* **2014**, *7*, 196–208. [CrossRef]
11. Renshaw, J.C.; Robson, G.D.; Trinci, A.P.J.; Wiebe, M.G.; Livens, F.R.; Collison, D.; Taylor, R.J. Fungal Siderophores: Structures, Functions and Applications. *Mycol. Res.* **2002**, *106*, 1123–1142. [CrossRef]

12. Hernlem, B.J.; Vane, L.M.; Sayles, G.D. The Application of Siderophores for Metal Recovery and Waste Remediation: Examination of Correlations for Prediction of Metal Affinities. *Water Res.* **1999**, *33*, 951–960. [CrossRef]
13. Li, Y.; Wei, S.; Chen, X.; Dong, Y.; Zeng, M.; Yan, C.; Hou, L.; Jiao, R. Isolation of Cadmium-Resistance and Siderophore-Producing Endophytic Bacteria and Their Potential Use for Soil Cadmium Remediation. *Heliyon* **2023**, *9*, e17661. [CrossRef]
14. Valverde-Sarmiento, C.; Espinosa-Iglesias, D.; Bautista-Toledo, M.I.; Álvarez-Merino, M.A.; Maldonado-Hódar, F.J.; Carrasco-Marín, F.; Pérez-Cadenas, A.F. Bacteria Supported on Carbon Films for Water Denitrification. *Chem. Eng. J.* **2015**, *259*, 424–429. [CrossRef]
15. Ehrhardt, H.M.; Rehm, H.J. Phenol Degradation by Microorganisms Adsorbed on Activated Carbon. *Appl. Microbiol. Biotechnol.* **1985**, *21*, 32–36. [CrossRef]
16. Benjedim, S.; Romero-Cano, L.A.; Pérez-Cadenas, A.F.; Bautista-Toledo, M.I.; Lotfi, E.M.; Carrasco-Marín, F. Removal of Emerging Pollutants Present in Water Using an E-Coli Biofilm Supported onto Activated Carbons Prepared from Argan Wastes: Adsorption Studies in Batch and Fixed Bed. *Sci. Total Environ.* **2020**, *720*, 137491. [CrossRef]
17. Figueiredo, J.L.; Pereira, M.F.R.; Freitas, M.M.A.; Órfão, J.J.M. Modification of the Surface Chemistry of Activated Carbons. *Carbon* **1999**, *37*, 1379–1389. [CrossRef]
18. Elmouwahidi, A.; Bailón-García, E.; Pérez-Cadenas, A.F.; Maldonado-Hódar, F.J.; Carrasco-Marín, F. Activated Carbons from KOH and H3PO4-Activation of Olive Residues and Its Application as Supercapacitor Electrodes. *Electrochim. Acta* **2017**, *229*, 219–228. [CrossRef]
19. Manikandan, S.K.; Pallavi, P.; Shetty, K.; Bhattacharjee, D.; Giannakoudakis, D.A.; Katsoyiannis, I.A.; Nair, V. Effective Usage of Biochar and Microorganisms for the Removal of Heavy Metal Ions and Pesticides. *Molecules* **2023**, *28*, 719. [CrossRef]
20. González-Díaz, R.L.; de Anda, J.; Shear, H.; Padilla-Tovar, L.E.; Lugo-Melchor, O.Y.; Olvera-Vargas, L.A. Assessment of Heavy Metals in Surface Waters of the Santiago–Guadalajara River Basin, Mexico. *Hydrology* **2025**, *12*, 37. [CrossRef]
21. Valdovinos-Flores, C. Industrialization and Its Environmental Impact on Health and Pollution in the Santiago River Basin of Mexico. *Int. J. Environ. Sci. Technol.* **2025**, *22*, 16247–16260. [CrossRef]
22. Hansen, A.M.; González-Márquez, L.C. Scenarios of Metal Concentrations in the Arcediano Dam (State of Jalisco, Mexico). *J. Environ. Sci. Health A Tox. Hazard. Subst. Environ. Eng.* **2010**, *45*, 99–106. [CrossRef]
23. Gómez-Meda, B.C.; Zúñiga-González, G.M.; Sánchez-Orozco, L.V.; Zamora-Perez, A.L.; Rojas-Ramírez, J.P.; Rocha-Muñoz, A.D.; Sobrevilla-Navarro, A.A.; Arellano-Avelar, M.A.; Guerrero-de León, A.A.; Armendáriz-Borunda, J.S.; et al. Buccal Micronucleus Cytome Assay of Populations under Chronic Heavy Metal and Other Metal Exposure along the Santiago River, Mexico. *Environ. Monit. Assess.* **2017**, *189*, 522. [CrossRef]
24. Shine, J.P.; Ryan, D.K.; Ford, T.E. Annual Cycle of Heavy Metals in a Tropical Lake-Lake Chapala, Mexico. *J. Environ. Sci. Health A Tox. Hazard. Subst. Environ. Eng.* **1998**, *33*, 23–43. [CrossRef]
25. Klučáková, M. The Effect of Supramolecular Humic Acids on the Diffusivity of Metal Ions in Agarose Hydrogel. *Molecules* **2022**, *27*, 1019. [CrossRef]
26. Sedláček, P.; Klučáková, M. Simple Diffusion Method Applied in Evaluation of Metal Transport in Model Humic Matrices. *Geoderma* **2009**, *153*, 11–17. [CrossRef]
27. Meza-González, D.A.; Gómez-Navarro, C.S.; Sandoval-García, K.; Zárate-Guzmán, A.I.; Zárate-Navarro, M.A.; Romero-Cano, L.A. Phytoremediation of Copper-Contaminated Water Using *Epipremnum aureum*: Adsorption Mechanisms and Continuous Flow Performance in Green Wall Systems. *Processes* **2026**, *14*, 100. [CrossRef]
28. Pamukoglu, M.Y.; Kargi, F. Batch Kinetics and Isotherms for Biosorption of Copper(II) Ions onto Pre-Treated Powdered Waste Sludge (PWS). *J. Hazard. Mater.* **2006**, *138*, 479–484. [CrossRef]
29. Rezaei, B.; Sadeghi, E.; Meghdadi, S. Nano-Level Determination of Copper with Atomic Absorption Spectrometry after Pre-Concentration on N,N-(4-Methyl-1,2-Phenylene)Diquinoline-2-Carboxamide–Naphthalene. *J. Hazard. Mater.* **2009**, *168*, 787–792. [CrossRef]
30. Madrid, Y.; Zayas, Z.P. Water Sampling: Traditional Methods and New Approaches in Water Sampling Strategy. *TrAC Trends Anal. Chem.* **2007**, *26*, 293–299. [CrossRef]
31. Madigan, M.T.; Bender, K.S.; Buckley, D.H.; Sattley, W.M.; Stahl, D.A. *Brock Biology of Microorganisms*; Pearson: London, UK, 2021; p. 1088.
32. Honsig, C.; Selitsch, B.; Hollenstein, M.; Vossen, M.G.; Spettel, K.; Willinger, B. Identification of Filamentous Fungi by MALDI-TOF Mass Spectrometry: Evaluation of Three Different Sample Preparation Methods and Validation of an In-House Species Cutoff. *J. Fungi* **2022**, *8*, 383. [CrossRef]
33. Schwyn, B.; Neilands, J.B. Universal Chemical Assay for the Detection and Determination of Siderophores. *Anal. Biochem.* **1987**, *160*, 47–56. [CrossRef]
34. de Anda-Rodríguez, F.A.; Corona-Ramírez, M.R.; Patiño-Arévalo, C.D.; Zárate-Navarro, M.A.; Zárate-Guzmán, A.I.; Romero-Cano, L.A. Mycomaterials from Agave Bagasse: A Valorization Strategy for Sustainable Tequila Packaging. *Fermentation* **2025**, *11*, 500. [CrossRef]

35. Andrews, M.Y.; Santelli, C.M.; Duckworth, O.W. Digital Image Quantification of Siderophores on Agar Plates. *Data Brief* **2016**, *6*, 890–898. [CrossRef]
36. Haijian, M.; Qiming, Q.; Xinyi, S. Shadow Segmentation and Compensation in High Resolution Satellite Images. In Proceedings of the International Geoscience and Remote Sensing Symposium (IGARSS), Boston, MA, USA, 7–11 July 2008; Volume 2. [CrossRef]
37. Siegel, J.P. The Mammalian Safety of *Bacillus thuringiensis*-Based Insecticides. *J. Invertebr. Pathol.* **2001**, *77*, 13–21. [CrossRef]
38. Romero-Cano, L.A.; García-Rosero, H.; Gonzalez-Gutierrez, L.V.; Baldenegro-Pérez, L.A.; Carrasco-Marín, F. Functionalized Adsorbents Prepared from Fruit Peels: Equilibrium, Kinetic and Thermodynamic Studies for Copper Adsorption in Aqueous Solution. *J. Clean. Prod.* **2017**, *162*, 195–204. [CrossRef]
39. *NOM-127-SSA1-2021*; Agua Para Uso y Consumo Humano. Límites Permisibles de la Calidad del Agua. Secretaría de Salud: Mexico City, Mexico, 2021. Available online: https://www.dof.gob.mx/nota_detalle_popup.php?codigo=5650705 (accessed on 18 December 2025).
40. *NOM-147-SEMARNAT/SSA1-2004*; Que Establece Criterios Para Determinar Las Concentraciones de Remediación de Suelos Contaminados por Arsénico, Bario, Berilio, Cadmio, Cromo Hexavalente, Mercurio, Níquel, Plata, Plomo, Selenio, Talio y/o Vanadio. SEMARNAT and the Ministry of Health: Mexico City, Mexico, 2004. Available online: https://www.profepa.gob.mx/innovaportal/file/1392/1/nom-147-semarnat_ssa1-2004.pdf (accessed on 18 December 2025).
41. Moura-Mendes, J.; Cazal-Martínez, C.C.; Rojas, C.; Ferreira, F.; Pérez-Estigarribia, P.; Dias, N.; Godoy, P.; Costa, J.; Santos, C.; Arrua, A. Species Identification and Mycotoxigenic Potential of Aspergillus Section Flavi Isolated from Maize Marketed in the Metropolitan Region of Asunción, Paraguay. *Microorganisms* **2023**, *11*, 1879. [CrossRef]
42. Sinha, A.K.; Parli, B.V. Siderophore Production by Bacteria Isolated from Mangrove Sediments: A Microcosm Study. *J. Exp. Mar. Biol. Ecol.* **2020**, *524*, 151290. [CrossRef]
43. Searle, L.J.; Méric, G.; Porcelli, I.; Sheppard, S.K.; Lucchini, S. Variation in Siderophore Biosynthetic Gene Distribution and Production across Environmental and Faecal Populations of *Escherichia coli*. *PLoS ONE* **2015**, *10*, 117906. [CrossRef]
44. Nithyapriya, S.; Lalitha, S.; Sayyed, R.Z.; Reddy, M.S.; Dailin, D.J.; El Enshasy, H.A.; Luh Suriani, N.; Herlambang, S. Production, Purification, and Characterization of Bacillibactin Siderophore of *Bacillus subtilis* and Its Application for Improvement in Plant Growth and Oil Content in Sesame. *Sustainability* **2021**, *13*, 5394. [CrossRef]
45. Upreti, R.; Thomas, P. Root-Associated Bacterial Endophytes from *Ralstonia solanacearum* Resistant and Susceptible Tomato Cultivars and Their Pathogen Antagonistic Effects. *Front. Microbiol.* **2015**, *6*, 129679. [CrossRef]
46. Hersman, L.E.; Huang, A.; Maurice, P.A.; Forsythe, J.H. Siderophore Production and Iron Reduction by Pseudomonas Mendocina in Response to Iron Deprivation. *Geomicrobiol. J.* **2000**, *17*, 261–273. [CrossRef]
47. Mokracka, J.; Koczura, R.; Kaznowski, A. Yersiniabactin and Other Siderophores Produced by Clinical Isolates of *Enterobacter* Spp. and *Citrobacter* Spp. *FEMS Immunol. Med. Microbiol.* **2004**, *40*, 51–55. [CrossRef]
48. Gopalakrishnan, S.; Humayun, P.; Kiran, B.K.; Kannan, I.G.K.; Vidya, M.S.; Deepthi, K.; Rupela, O. Evaluation of Bacteria Isolated from Rice Rhizosphere for Biological Control of Charcoal Rot of Sorghum Caused by *Macrophomina phaseolina* (Tassi) Goid. *World J. Microbiol. Biotechnol.* **2011**, *27*, 1313–1321. [CrossRef]
49. Rabbee, M.F.; Sarafat Ali, M.; Choi, J.; Hwang, B.S.; Jeong, S.C.; Baek, K. *Bacillus velezensis*: A Valuable Member of Bioactive Molecules within Plant Microbiomes. *Molecules* **2019**, *24*, 1046. [CrossRef]
50. Bendaha, M.E.A.; Belaouni, H.A. Tomato Growth and Resistance Promotion by *Enterobacter Hormaechei* subsp. *Steigerwaltii* EB8D. *Arch. Phytopathol. Plant Prot.* **2019**, *52*, 318–332. [CrossRef]
51. Saber, F.M.A.; Abdelhafez, A.A.; Hassan, E.A.; Ramadan, E.M. Characterization of Fluorescent Pseudomonads Isolates and Their Efficiency on the Growth Promotion of Tomato Plant. *Ann. Agric. Sci.* **2015**, *60*, 131–140. [CrossRef]
52. Drechsel, H.; Thieken, A.; Reissbrodt, R.; Jung, G.; Winkelmann, G. α-Keto Acids Are Novel Siderophores in the Genera Proteus, Providencia, and Morganella and Are Produced by Amino Acid Deaminases. *J. Bacteriol.* **1993**, *175*, 2727–2733. [CrossRef]
53. Namikawa, H.; Niki, M.; Niki, M.; Oinuma, K.I.; Yamada, K.; Nakaie, K.; Tsubouchi, T.; Tochino, Y.; Takemoto, Y.; Kaneko, Y.; et al. Siderophore Production as a Biomarker for *Klebsiella pneumoniae* Strains That Cause Sepsis: A Pilot Study. *J. Formos. Med. Assoc.* **2022**, *121*, 848–855. [CrossRef]
54. Wilson, M.K.; Abergel, R.J.; Raymond, K.N.; Arceneaux, J.E.L.; Byers, B.R. Siderophores of *Bacillus anthracis*, *Bacillus cereus*, and *Bacillus thuringiensis*. *Biochem. Biophys. Res. Commun.* **2006**, *348*, 320–325. [CrossRef]
55. Nowak, B.; Chlebek, D.; Hupert-Kocurek, K. *Priestia megaterium* KW16: A Novel Plant Growth-Promoting and Biocontrol Agent Against *Rhizoctonia solani* in Oilseed Rape (*Brassica napus* L.)—Functional and Genomic Insights. *Agriculture* **2025**, *15*, 1435. [CrossRef]
56. Prajakta, B.M.; Suvarna, P.P.; Raghvendra, S.P.; Alok, R.R. Potential Biocontrol and Superlative Plant Growth Promoting Activity of Indigenous *Bacillus mojavensis* PB-35(R11) of Soybean (*Glycine max*) Rhizosphere. *SN Appl. Sci.* **2019**, *1*, 1143. [CrossRef]
57. Sunar, K.; Dey, P.; Chakraborty, U.; Chakraborty, B. Biocontrol Efficacy and Plant Growth Promoting Activity of Bacillus Altitudinis Isolated from Darjeeling Hills, India. *J. Basic Microbiol.* **2015**, *55*, 91–104. [CrossRef]

58. Gomaa, E.Z.; El-Meihy, R.M. Bacterial Biosurfactant from Citrobacter Freundii MG812314.1 as a Bioremoval Tool of Heavy Metals from Wastewater. *Bull. Natl. Res. Cent.* **2019**, *43*, 69. [CrossRef]
59. Rudakova, N.L.; Khilyas, I.V.; Danilova, I.V.; Pudova, D.S.; Sharipova, M.R. Evaluating of the Potential of Bacillus Pumilus 3-19 as a Plant Growth-Promoting Strain. *Russ. J. Plant Physiol.* **2023**, *70*, 197. [CrossRef]
60. Wang, D.; Zhan, Y.; Cai, D.; Li, X.; Wang, Q.; Chen, S. Regulation of the Synthesis and Secretion of the Iron Chelator Cyclodipeptide Pulcherriminic Acid in *Bacillus licheniformis*. *Appl. Environ. Microbiol.* **2018**, *84*, e00262-18. [CrossRef]
61. Liu, G.; Li, X.; Lee, J.W.; Popov, B.N. A Review of the Development of Nitrogen-Modified Carbon-Based Catalysts for Oxygen Reduction at USC. *Catal. Sci. Technol.* **2011**, *1*, 207–217. [CrossRef]